Quaternary Science Reviews 337 (2024) 108800

Contents lists available at ScienceDirect

Quaternary Science Reviews

journal homepage: www.elsevier.com/locate/quascirev

High-resolution relative paleointensities over the last 40 ka from marine sediments in the western equatorial pacific: Magnetic events and interhemispheric correlation

Dauchy-Tric Louise [a,*], Carlut Julie [a], Bassinot Franck [b], Valet Jean-Pierre [a]

[a] Université Paris Cité, Institut de Physique du Globe de Paris, CNRS UMR-7154, 1 rue Jussieu, Paris Cedex 05, France
[b] LSCE/IPSL, CEA-CNRS-UVSQ, Université Paris-Saclay, Gif-sur Yvette, France

ARTICLE INFO

Handling Editor: Mira Matthews

Keywords:
Western equatorial pacific
Relative paleointensity
Geomagnetic excursions
Lock-in depth

ABSTRACT

Core MD01-2385 retrieved in the western equatorial Pacific (Northwest of Papua-New Guinea) has been sampled every 2 cm for paleomagnetic and radiocarbon measurements. The age model, well constrained by 47 ^{14}C ages (both new and former), indicates that our record spans approximately the last 38 ka. The average sedimentation rate is ~30 cm/ka. Analysis of the magnetic mineralogy revealed that the natural remanent magnetization (NRM) is predominantly carried by magnetite. A relative paleointensity record (RPI) was derived, allowing us to estimate a lock-in depth of approximately 18 cm, corresponding to ~600 years in our case, by comparing it with the CALS10k.2 model. Comparison with two other western Equatorial Pacific RPI, selected for their geographical proximity (~1000 km) and high resolution, allowed us to compile a regional reference record (WEPEQ). Several intervals of lower intensities have been identified and may correspond to the known events of Mono Lake (~34 ka), Rockall (~27 ka), Hilina Pali (~18 ka) and possibly Tianchi (~5–8 ka). Overall, our equatorial curve exhibits strong similarities with RPI curves from mid to low latitudes, such as those from the Iberian Margin and Black Sea. A detailed investigation hints at the presence of non-dipolar structures in the Earth's magnetic field at the shorter time scale, especially during the low intensity intervals. In contrast, notable differences are observed when compared to high-latitude stacks, especially from the North Atlantic (NAPIS). This points to the potential climatic bias that may affect high-latitude records during the glacial maximum and glacial-interglacial transition.

1. Introduction

The continuous variations in the paleointensity of the Earth's magnetic field are mostly known from the study of marine sediments, which, in favorable cases (e.g. Tauxe, 1993), provide a record of the field's evolution. The vast majority of ocean sediments have an accumulation rate of less than 10 cm/ka (e.g. Olson et al., 2016). In such cases the time interval between two adjacent samples is usually of a few hundreds to thousand years and the paleointensity variations are smoothed to a large extent. When variations of the Earth magnetic field span more than a few thousand years, they are believed to reflect essentially variations in the dipole's intensity, with very moderate non dipole contributions (e.g. Carlut et al., 2000). This is attested by the strong similarities observed between the sediment-derived paleointensity records from very different regions and the global virtual axial dipole moment (VADM) whose variations have been compiled for time periods ranging from the last 800 ka up to 2 million years (Guyodo and Valet, 1999; Valet et al., 2005; Channell et al., 2009; Laj et al., 2013).

In addition to global variations, regional reference curves were produced for shorter time intervals (less than 80 ka) using the combination of marine records with high sedimentation rates (i.e. above 10 cm/ka) from specific areas: the North Atlantic with NAPIS (La j et al., 2000), the South Atlantic with SAPIS (Stoner et al., 2002), the Black Sea with the Black Sea Stack (Liu et al., 2020) and the Iberian Margin with the Iberian Margin Stack (Channell et al., 2018). In theory, these records could integrate local, non-dipole, structure of the earth magnetic field, making them of great interest for the study of short events (e.g. excursions), and geodynamo modelings.

Comparisons between these curves show an overall consistency of paleointensity variations, except for the last 30 ka, where significant disparities have been observed, particularly between NAPIS and SAPIS. For instance, a maximum intensity is observed on NAPIS at ~25 ka,

* Corresponding author.
E-mail address: dauchy@ipgp.fr (D.-T. Louise).

https://doi.org/10.1016/j.quascirev.2024.108800
Received 4 May 2024; Received in revised form 22 June 2024; Accepted 23 June 2024
Available online 9 July 2024

while SAPIS shows a minimum intensity at the same period. Stoner et al. (2002) put forward several hypotheses to explain these inter-hemispheric differences, such as dating and temporal correlation problems over the past 30 kyr interval, the existence of a strongly non-dipolar component, or the presence of uncorrected climatic and environmental biases.

Several studies also reported excursions associated with changes in direction and/or drops in intensity of the Earth's magnetic field (Mono Lake at ~34 ka, Rockall at ~26 ka, Hilina Pali at ~19 ka, Gothenburg at ~13 ka, Tianchi excursion at ~ 10 ka). The reliability of many of them is still debated as they are not systematically observed (Channell et al., 2020; Simon et al., 2020). These "excursions" could correspond to local features due to non dipolar terms or recording distortions, explaining why they are not detected at a global scale.

Thus, the most recent, continuous and detailed records of the Earth's magnetic field have raised questions regarding the mechanisms that drive variations in paleointensity records, even for recent geological times as the Holocene. This demonstrates that we still have an incomplete understanding of the small scale variations of the field. However, acquiring new high resolution paleomagnetic records to investigate the different hypotheses is not straightforward. The highest oceanic sedimentation rates are often associated with areas of high primary productivity, resulting in significant fluxes of organic carbon into marine sediments, which usually drive an intense reductive diagenesis and the dissolution of magnetic minerals, erasing the magnetic signal (Larrasoaña et al., 2003). Sedimentation rates are closely linked to (1)

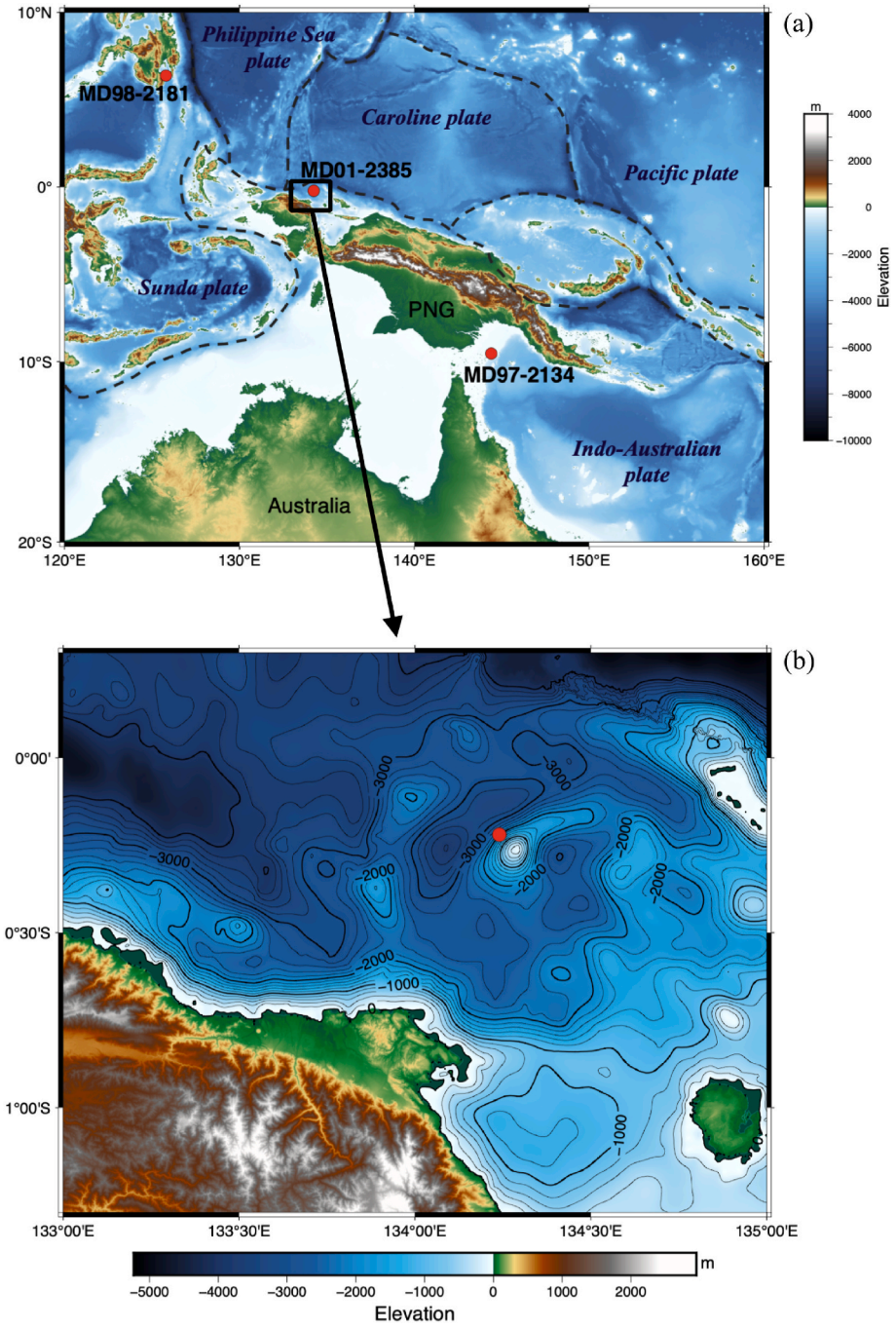

Fig. 1. (a) Bathymetric map of the western equatorial Pacific with the location of the core used in this study. Plate boundaries are indicated by dotted lines. (b) Bathymetric map of the area around core MD01-2385 (red dot). Intervals of bathymetric contours are 200 m. PNG = Papua-New Guinea.

erosion and the supply of terrigenous material and, (2) sedimentary process associated with bottom current intensity (i.e. the focusing or removal of fine particles), so that fine climatic variations are also expected to have an influence on cores with high sedimentation rates. Hence, detailed age models are essential for the robust comparisons of datasets. This requires the acquisition of multiple independent radiometric ages.

In this study, novel high-resolution relative paleointensity and ^{14}C age data spanning the past 38 kyr have been acquired for core MD01-2385 located in the Papua-New Guinea region. Limited diagenesis, and a high sedimentation rate, combined with our high-resolution sampling strategy (i.e. data points averaging approximately ~60–70 years), have allowed the construction of an exceptionally detailed paleointensity curve. The consistency observed between successive data points underscores a robust temporal correlation of paleointensity at this resolution. By stacking our magnetic records with locally derived high-resolution curves, we generated a composite paleointensity record for the region.

2. Material & methods

2.1. Geographical and tectonical setting

Core MD01-2385 (0.22 S, 134.24 E; 2602 m water depth) was retrieved on the northwest margin of the Papua-New Guinea, north of the Bird's Head Peninsula, during the R/V Marion Dufresne IMAGES VII cruise in 2001. This 32.46 m long core was collected using the giant piston corer (GPC) and then cut into 1.5 m long sections on board. Papua-New Guinea lies at the boundary between several tectonic plates including the Sunda plate to the west (part of the Eurasian plate), the Indo-Australian plate to the south, the Pacific-Caroline plate to the northeast and the Philippine Sea plate to the northwest, making this region a rather tectonically complex spot with a combination of compressive, extensive, and strike-slip movements (Baldwin et al., 2012). However, the core MD01-2385 is situated in a relatively quiet area with fewer earthquakes compared with eastern Papua New Guinea (Baldwin et al., 2012), and no nearby volcanoes (Orynbaikyzy et al., 2023). It is surrounded by a semi-circular bathymetric high (Fig. 1). In addition, the sediment consists of rather homogenous brownish clays, with no major changes observed between sediments deposited during glacial and interglacial periods. All these elements make the MD01-2385 core a judicious choice as an undisturbed reference core for the region (Fig. 1).

2.2. Magnetic measurements

Core MD01-2385 was sampled at high resolution using adjacent 8 cm^3 paleomagnetic cubes carefully pushed into the sediment. The first step consisted of measuring the magnetic susceptibility with a AGICO KLY-3.

The natural remanent magnetization (NRM) of each sample was measured at 11 steps of alternating field (AF) demagnetization (10, 15, 20, 25, 30, 35, 40, 50, 60, 70 and 90 mT) using a LDA-3 and 2G 755-HR cryogenic magnetometer. The anhysteretic remanent magnetization (ARM) was acquired in a 100 mT demagnetization field with a 0.05 mT steady field. The ARM was then AF demagnetized at peak fields of 20, 30 and 40 mT. The anhysteretic susceptibility ($Karm_{20}$) was calculated according to the following equation

$$Karm_{20} = \frac{ARM_{20}}{0.05} \quad (1)$$

with ARM_{20} corresponding to the ARM measured after the AF demagnetization at 20 mT.

Isothermal remanent magnetization (IRM) was applied in a 1 T direct field (IRM_{1T}) and a 0.3 T backfield ($IRM_{-0.3T}$), enabling to determine the S-ratio, corresponding to the IRM-0.3_T/IRM1 $_T$ ratio. The IRM acquired at 1 T is referred to here as the saturation IRM (SIRM). For a series of 84 samples IRM acquisitions were performed with a 2.5 T field, the measured values and variations observed were nearly identical to those obtained with a 1 T direct field.

The temperature-dependance of magnetic susceptibility was measured with the same instrument used for magnetic susceptibility, coupled with a CS-3 heating unit and up to ~630 °C from powder extract from 10 representative depth levels along the core.

2.3. ^{14}C dating

Nine ^{14}C dating points have been measured by Wu et al. (2017) with a maximum age of 29.255 cal ka BP at a core depth of 870–872 cm (Table 1). However, two of the ^{14}C ages result in a reversal in the age model (Table 1). In order to obtain a more robust and detailed age

Table 1
^{14}C dates of planktonic foraminifera *G.ruber*, *G. sacculifer* and *G.trilobus* from core MD01-2385 (see section 2.3 for details). Depths marked with an asterisk (*) correspond to dates from Wu et al. (2017). All dating carried out for this study were performed on the UMS-ARTEMIS (Pelletron 3 MV) AMS (CNRS-CEA Saclay, France).

Depth core (cm)	Depth corrected (cm)	Original 14C date (yr)	±1σ	Calendar date (yr BP)	+1σ	-1σ
30-32 *	30–32	1040	30	579	461	689
79.5–81	79.5–81	2555	30	2207	2024	2352
139–141	139–141	4395	30	4517	4324	4729
150–151.5 *	150–151.5	4005	35	3999	3817	4203
210–211.5 *	210–211.5	5155	45	5451	5276	5607
270–271.5	270–271.5	7610	30	8014	7864	8169
360-362 *	360–362	9320	44	10115	9887	10287
390–391.5	390–391.5	10135	35	11220	11053	11411
410–411	410–411	10280	35	11413	11211	11649
440-442 *	440–442	10977	48	12478	12240	12663
450–452	450–452	10600	35	11916	11678	12187
490-492 *	490–492	12220	58	13702	13492	13953
540–542	540–542	13095	45	15064	14827	15295
570–571	570–571	14245	45	16560	16297	16837
580–582	580–582	13980	45	16216	15968	16478
600–602	600–602	18140	70	21142	20834	21457
621–624	621–624	14505	50	16884	16608	17125
659-661 *	659–661	15204	57	17748	17432	18032
670–672	670–672	13660	45	15803	15550	16056
680–681.5	680–681.5	15390	50	17975	17729	18200
719-721 *	719–721	14842	67	17276	16999	17603
730–731.5	730–731.5	16420	60	19058	18813	19338
750–752	750–752	15730	50	18343	18125	18603
820–822	820–822	17290	70	20131	19849	20408
830–831	830–831	19720	80	22954	22660	23240
850–852	850–852	18710	70	21907	21593	22186
859.5–861	859.5–861	20750	90	24072	23780	24403
870-872 *	870–872	25758	147	29255	28883	29694
875–877	875–877	24650	140	28081	27727	28491
878–880	878–880	27040	160	30510	30121	30873
910–911	890–891	21890	100	25414	25111	25702
940–941	920–921	23380	120	26923	26509	27205
1000–1001	980–981	22690	110	26143	25847	26438
1040–1041	1020–1021	23750	180	27251	26900	27633
1080–1081	1060–1061	25600	150	29073	28706	29507
1100–1101	1080–1081	26820	160	30293	29960	30712
1120–1121	1100–1101	27590	190	30991	30605	31366
1140–1141	1120–1121	28630	200	32046	31516	32786
1160–1161	1140–1141	29360	230	33090	32273	33719
1180–1181	1160–1161	29400	220	33149	32377	33759
1200–1201	1180–1181	29770	230	33577	33021	34109
1220–1221	1200–1201	32300	510	36059	34939	37258
1240–1241	1220–1221	31370	310	35084	34438	35774
1260–1261	1240–1241	33050	330	36874	36084	37781
1280–1281	1260–1261	33530	340	37532	36588	38611
1300–1301	1280–1281	32050	310	35784	35141	36435
1320–1321	1300–1301	33260	360	37158	36239	38251

model, new ^{14}C dating were performed on this core, adding 38 points. The measurements were carried out on samples consisting only of the planktonic foraminifera species *Globigerinoides ruber*, except for the sample at 79.5–81 cm where *Globigerinoides trilobus* was combined with *G. ruber* to have enough material. The calibration of the ^{14}C ages and the age-depth relationship were made using Bacon Software (Blaauw and Christen, 2011). The regional difference from the average modern global marine reservoir effect (ΔR), was estimated using CALIB v8.2 (Stuiver and Reimer, 1993). ΔR is 123 ± 28 years. The core depth was corrected below 880 cm to take into account a sediment slippage which occurred during the corer pulling out, resulting in a void space between 880 and 900 cm.

3. Results

3.1. Magnetic properties

A well defined ChRM direction was isolated for the vast majority of samples using 7 to 11 demagnetization steps (typically between 15 and 90 mT). The ChRM directions (declination and inclination) of each sample and their associated uncertainties are represented in Fig. 2. The magnetization components are well-defined as suggested by low MAD (<4°) values. Inclination values are close to those expected at this latitude (~0°) and reconstructed declination depicts smooth variations with indications of a very gradual rotation of the core inside the core barrel between 700 and 1050 cm (Stoner et al., 2000; Channell, 2013). The medium destructive field (MDF) of the NRM lies between 25 and 35 mT (Fig. 2) except for the 750–850 cm interval, where MDF values are higher, around 40–45 mT. This can be explained by the presence of significant viscous reverse magnetization removed after AF demagnetization at 10–15 mT (Fig. 3c and d).

The S-ratio (Fig. 4g) is remarkably constant with values ranging from 0.96 to 0.99 and indicates that the magnetization is mostly carried by low-coercivity minerals such as magnetite. The presence of magnetite is also confirmed by the temperature-dependence curves of magnetic susceptibility, with a drop at ~580 °C on heating curves (red curves on Fig. S1), which corresponds to the Curie temperature of magnetite. These observations indicate that NRM is predominantly carried by magnetite, which is an essential criteria for the use of marine sediments in RPI reconstruction (Tauxe, 1993).

Variations of K and SIRM show similar trends over the entire depth. Intervals of lower values are observed between 400 and 450 cm, 550–600 cm and 650–750 cm depth, and mirrored in the ARM_{20} data (Fig. 4). This is interpreted as reflecting a slightly lower concentration of

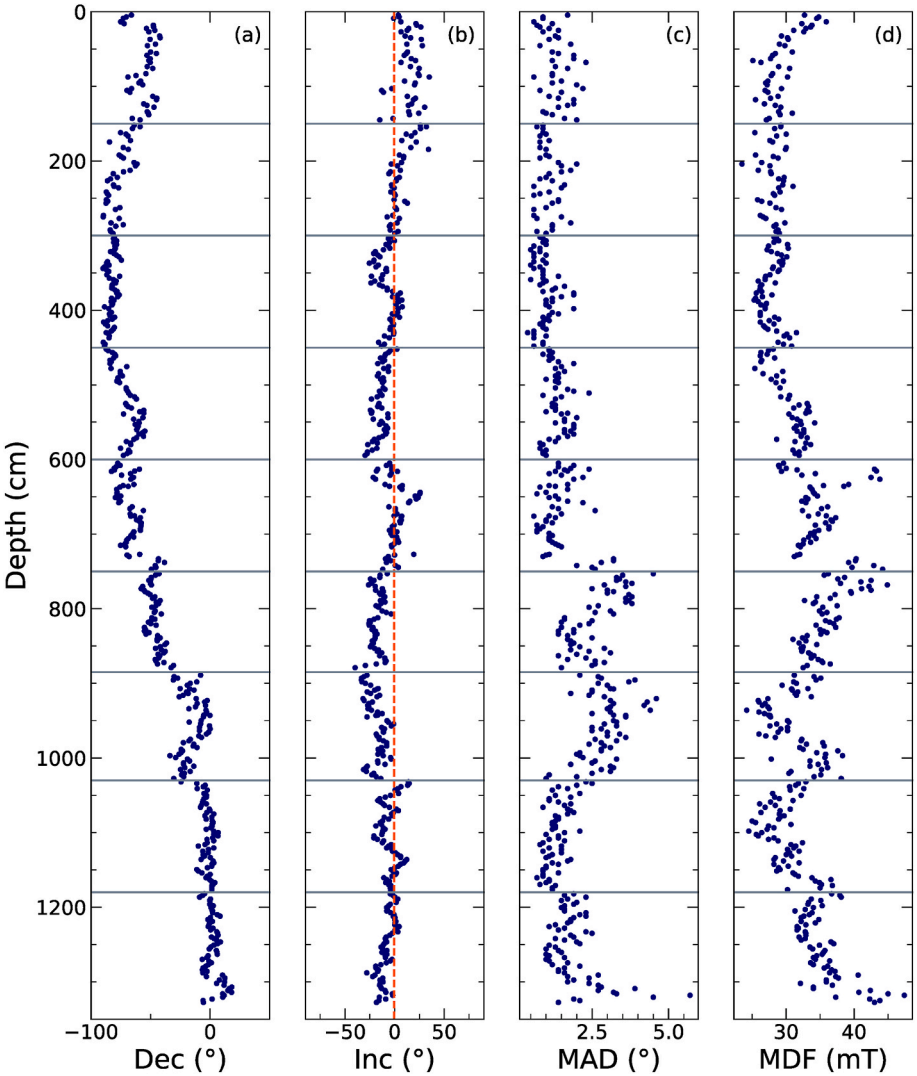

Fig. 2. (a) Declination (Dec), (b) inclination (Inc), (c) associated maximum angular deviation (MAD) and (d) medium destructive field (MDF) for each demagnetized sample. Declination values have been corrected by ~90° so that they can be represented centered on 0 for the deepest part. Gray lines represent boundaries between adjacent 1.5 m long sections. The orange dashed line represents the expected inclination value at the latitude of core site MD01-2385.

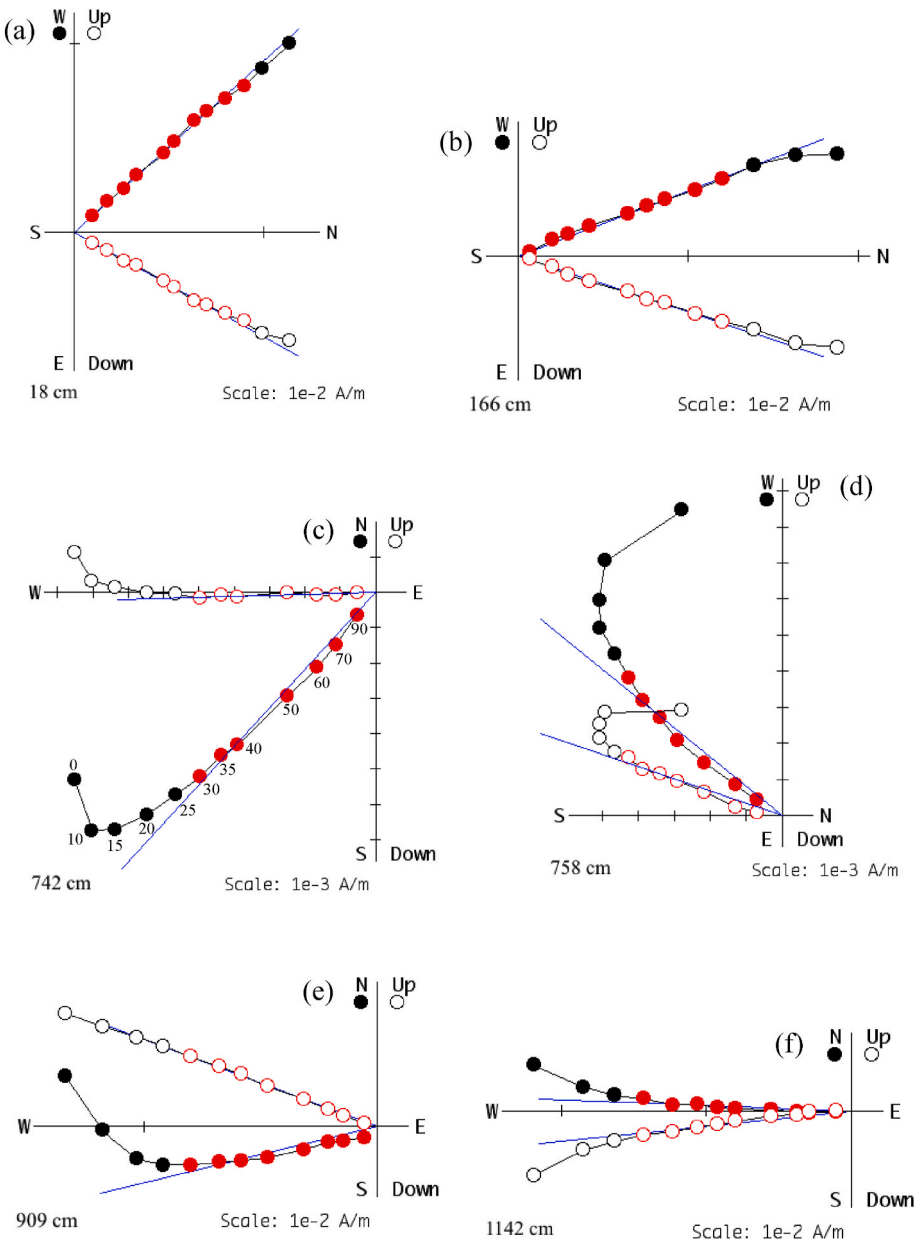

Fig. 3. Examples of orthogonal projection of natural remanent magnetization (NRM) during AF demagnetization for some cubes sampled from core MD01-2385. (c) Numbers indicate the alternating field in mT. The steps are the same for each orthogonal projection.

magnetic grain at these depths. The high values observed around 850 and 900 cm in both K and SIRM, along with an opposite trend on the ARM_{20} are discussed below. Despite some variations, the magnetic grain concentration remains in the same order of magnitude throughout the core, making it suitable for paleomagnetic study.

The magnetic granulometry variations, represented by the $Karm_{20}/K$ ratio (Fig. 4e), reveal three main trends. A trend toward low $Karm_{20}/K$, characteristic of larger grains, is observed from the bottom of the core up to ~600 cm. From this depth upward, $Karm_{20}/K$ ratio increases, indicating that the size of the magnetic grains gradually decreases, until a depth of ~350 cm from which it stabilizes with rather fine particles. High frequency oscillations are observed above 300 cm, resulting from the occurrence of decimetric thick events. The occurrence of coarse magnetic grains between 850 and 900 cm is attested by a low $Karm_{20}/K$ ratio and distinctive data points in the $Karm_{20}$ vs. K diagram. (Fig. 5). This interval is also marked by a peak of high K and SIRM, suggesting a higher concentration of magnetite.

Overall, the magnetic mineralogical and granulometric characteristics of core MD01-2385 correspond to the criteria proposed by Tauxe (1993) for the obtention of reliable paleointensities.

3.2. *Relative paleointensity (RPI)*

To reconstruct the RPI, it is necessary to normalize the NRM intensity by a parameter that effectively captures fluctuations in the sediment's magnetization capacity. Normalization by a laboratory-induced magnetization activating the same grains as those responsible for NRM makes it possible to correct part of the bias induced by changes in concentration and grain-size (Levi and Banerjee, 1976; Tauxe, 1993). Laboratory-induced remanent magnetizations such as the ARM or IRM are commonly used (Channell et al., 2018; Liu et al., 2020; Goto et al., 2024). In this study, RPI proxies were determined by normalization of NRM intensity by ARM intensity obtained at 20, 30 and 40 mT AF demagnetization steps. RPIs are determined either by calculating the

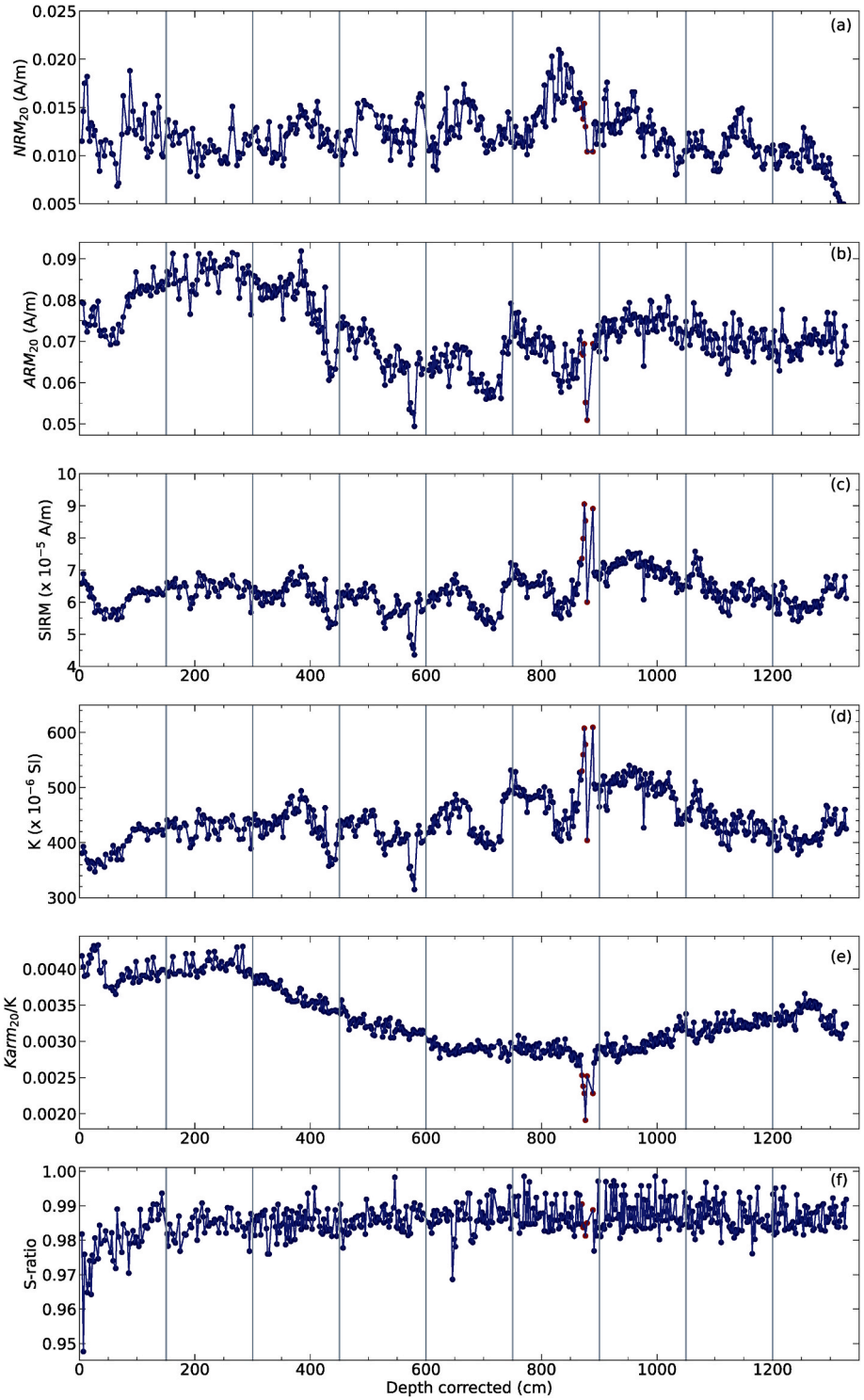

Fig. 4. Magnetic parameters as a function of corrected depth (cm): (a) NRM after 20 mT AF demagnetization, (b) ARM after 20 mT AF demagnetization, (c) the SIRM acquired at 1 T, (d) the susceptibility (K), (e) the ratio of anhysteretic susceptibility ($Karm_{20}$) over K, (f) the S-ratio determined as the ratio of $IRM_{-0.3T}$ over IRM_{1T}. Gray lines represent boundaries between adjacent 1.5 m long sections.

mean or the slope (using a linear regression) of the NRM_{20}/ARM_{20}, NRM_{30}/ARM_{30} and NRM_{40}/ARM_{40} ratios. The results obtained by these two different methods are undistinguishable and the RPI proxy defined by the slope between the NRM/ARM ratios will be used subsequently (Fig. 6). This RPI curve was compared with magnetic parameters that could be used as environmental proxies in order to assess the potential effects of environmental variations on paleointensity data acquisition. No correlation was observed between the curves (Fig. S2).

The RPI curve obtained shows variations with maximum intensity at ~830 cm, while minimum intensity values are obtained for the deepest part sampled, ie. from 1250 to 1350 cm (Fig. 6). Other intensity minima can be identified, such as those visible at ~225, 340, 450, 550, 625, 770 and 1100 cm.

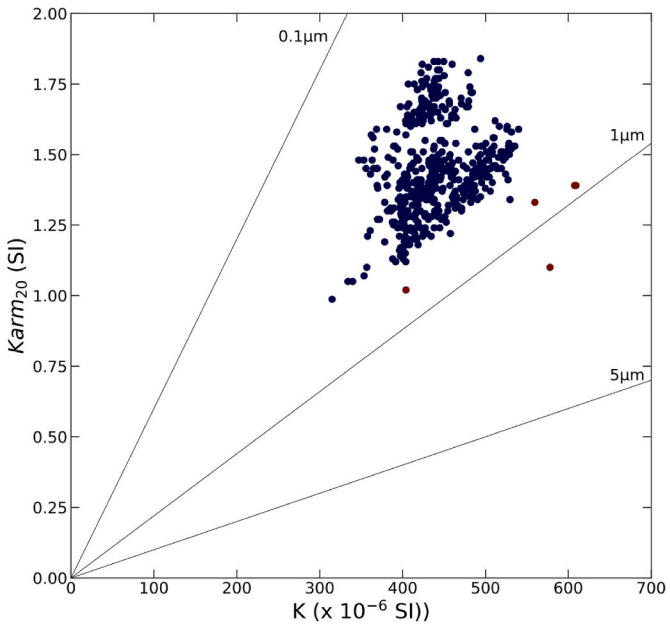

Fig. 5. Plot of anhysteretic susceptibility (Karm20) vs susceptibility (K) with magnetic grain size reference lines (King et al., 1983).

4. Chronological reconstruction

The acquisition of a very large number of ^{14}C dates over a short time interval makes it possible, on the one hand, to record very fine variations in the rate of sedimentation, and on the other hand, the existence of small remobilized zones. The ^{14}C results, listed in Table 1, are very consistent, resulting in smooth variations in the depth-age diagram. A few age inversions, not within the 2σ confidence interval, are present, particularly between ages obtained by Wu et al. (2017) and adjacent dates (less than 15 cm apart) obtained for this study. These inversions are generally of the order of 500 years and may be due to the use of different instruments in different laboratories and/or the use of different foraminifera species.

A marked unconformity can be observed between 870 and 880 cm depth. For the deepest interval, our calibrated ages of ~28 cal ka BP and ~30.5 cal ka BP, measured at 875–877 cm and 878–880 cm respectively, match well with the age of ~29 cal ka BP obtained at 870–872 cm by Wu et al. (2017) but are significantly older than the ages that bracket them. These anomalously old ages correspond to the depth at which a high concentration of coarse magnetite was identified (as revealed by the high K, IRM and ARM_{20} values found between 870 and 889 cm). The discrepancy is approximately 5 ka between the age of sample 878–880 cm and the adjacent ones. This may indicate the remobilization of older foraminifers during sediment deposition, and we assume that it may be representative of an instantaneous reworking event. The associated paleomagnetic results are discarded in the further course of this work. Another ^{14}C inversion on the order of a +4 ka is also observed at 600–602 cm. As there are no elements that suggest a problem with the 14C analysis itself, one can only assume that this anomalously old sediment interval contains reworked material. A last age inversion is observed at 670–672 cm. This inversion is more puzzling to interpret as it corresponds to an anomalously younger age. Previous studies have shown that the regional differences from the global marine reservoir effect can vary through time (Franke et al., 2008). However, the single-interval 14C anomaly at 670–672 cm corresponds to an unrealistic drop of ~2 ka in an area where modern regional reservoir age anomaly is −123 years, allowing us to reject the possibility that this anomaly is related to a change in the local reservoir age. In the rest of this paper, the anomalous 14C dates at 600–602 and 670–672 cm were considered as outliers (shown in light gray in Fig. 7).

The age model deduced from these ^{14}C dates gives an average sedimentation rate of ~28 cm/ka for the 38–20 ka interval and of ~35 cm/ka over the last 20 ka (Fig. 7), making MD01-2385 an outstanding candidate for high-resolution RPI and rock magnetic studies with well dated measurements point every 60–70 years.

5. Construction of a time dependent RPI stack for the western equatorial pacific

The 47 ^{14}C ages measured on our core attest to a high and rather regular sedimentation rate, enabling us to calibrate our RPI curve very precisely over time. The RPI data exhibits a robust temporal correlation, and, since our analysis is based solely on individual samples, the correlation between samples is not attributed to data smoothing but rather reflects Earth's magnetic field behavior. In particular, high and low value intervals are described by sets of 5–10 consecutive samples. With the calculated accumulation rate of 60–70 years per sample, the correlation time would typically be on the order of 350–700 years. With such coherent and long term variations we expect to find strong similarities between nearby records, provided that they are also of high temporal resolution and quality.

Spatial and temporal correlation of paleointensity variations was studied by Korte et al. (2019a) using Holocene geomagnetic field models variations (CALS10k.2). Model predictions for the VADM (intensity) at a given arbitrary location (54°N, −4°W, United Kingdom) were compared to model predictions to the N, S, E, and W of the site and

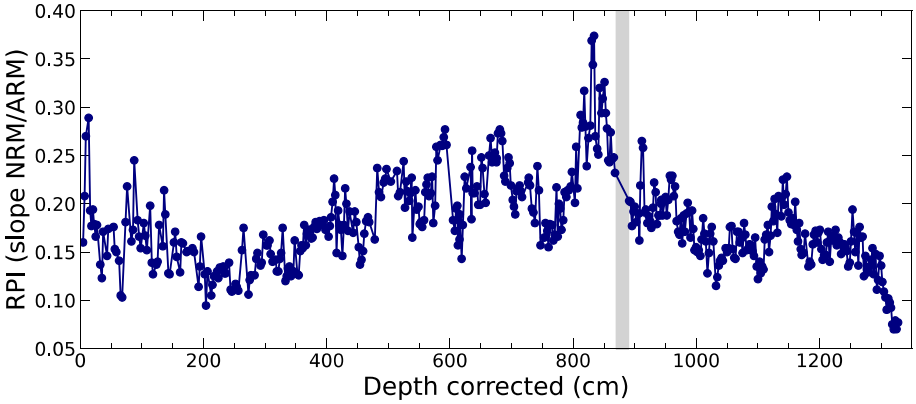

Fig. 6. Proxy of relative paleointensity (RPI) obtained for core MD01-2385 by calculating the slope between the NRM/ARM ratios at 20,30 and 40 mT AF demagnetization. The gray bar corresponds to the depth interval with coarse magnetic grains mentioned in section 3.1. The samples belonging to this interval have been removed from the relative paleointensity curve for reasons discussed in section 4.

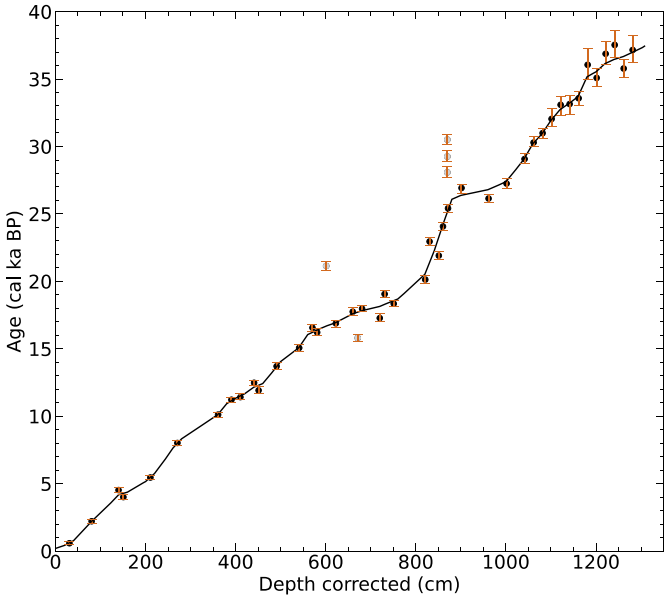

Fig. 7. Chronostratigraphy of core MD01-2385. The depth scale is corrected for the 20 cm slip and the 20 cm remobilization. Age/depth relationship was obtained with the Bacon Software (Blaauw and Christen, 2011). Dots represent the calibrated 14C ages. Those in light gray are considered as outliers (see section 4 for further details).

at 500, 1000, 2000, and 4000 km distances. Results show that VADM variations are almost indiscernible at and below 1000 km distance but differences between the records increase with distance with predictions

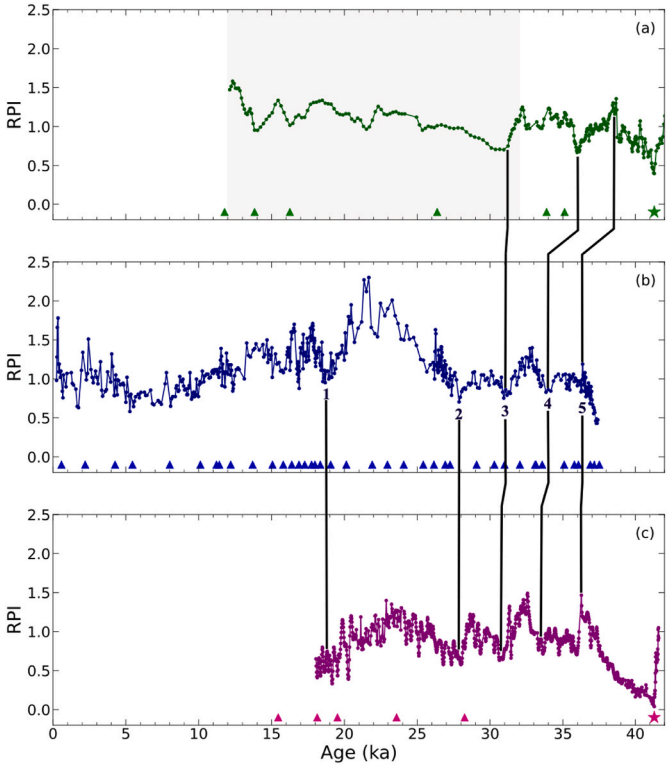

Fig. 8. Relative paleointensity data obtained from (a) core MD97-2134 by Blanchet et al. (2006), (b) core MD01-2385 and (c) MD98-2181 by Lund et al. (2017) on their respective age model. (a) The gray interval for MD97-2134 indicates sedimentation rate lower than 10 cm/ka, corresponding data are not considered. Triangles represent calibrated ^{14}C ages and stars represent the tie point associated with the Laschamp excursion.

starting to differ at 2000 km (Fig. 8 in Korte et al., 2019a). Our RPI curve was thus compared to other RPI located at less than 2000 km from our site. We selected records based on (1) the reliability of the paleomagnetic data determined in the laboratory which must be based, at least partly, on individual "cube" samples and paleointensity normalized by IRM or ARM, (2) high accumulation rates in order to be comparable with ours, and (3) multiple and accurate ^{14}C ages assigned to the data. Only two records match the selection criteria and provide high-resolution relative paleointensity over the last 40 ka in the selected area. The selected studies are Blanchet et al. (2006) with core MD97-2134 (southeast of the Papua-New Guinea margin at 9.9°S, 144.66°E, 760 m water depth), and Lund et al. (2017) with core MD98-2181 retrieved from the Devao Gulf, Philippine Islands (6.4°N, 125.8°E, 2114 m water depth). These two cores are ~1110 and 1250 km away from core MD01-2385, respectively. Both studies used a combination of u-channels and paleomagnetic cubes.

The Laschamps excursion is recorded around 41 ka in both cores MD97-2134 and MD98-2181, while only the subsequent increase in intensity is partly visible in the record of core MD01-2385. Well recognizable features are common to all three cores and numbered 3, 4 and 5 in Fig. 8. Two additional, more open to discussion, intensity minima, at ~20 ka and ~28 ka, can be correlated between the RPI curves of cores MD98-2181 and MD01-2385. The correlations proposed for features 1 and 2 could be subject to adjustment, given that they are marked by a wider intensity minima on the MD98-2181 core record compared with that of core MD01-2385. A positive point is that, based on the available ^{14}C-dated age models, the two features are quite well aligned in time between the curves. We therefore relied on the ^{14}C data and correlated these features without shifting them in time.

These observations suggest that all three curves for the selected time interval are representative of paleointensity variations of the geomagnetic field in this region despite some moderate time lags between the correlated structures. The differences can be explained by factors such as lock-in depth, which is very rarely corrected and varies from core to core, and by dating uncertainties.

In order to construct a stacked RPI, the curves were normalized by their mean intensity value between 32 and 37 ka, a period common to all three curves. A peak-to-peak correlation was performed between these three RPI curves, based on the MD01-2385 age model. Since the Laschamp excursion was extensively studied and precisely dated at 41.3 ka (Channell et al., 2017; Laj et al., 2014), its associated intensity minimum was used as our oldest tie-point (represented by stars in Fig. 8a and c), making it possible to accurately date the base of core MD98-2181 and MD97-2134 records prior to the stacking procedure. Our final West Pacific Equatorial (WEPEQ) reference curve is obtained by calculating the arithmetic mean of the RPI curves following the method described by Guyodo and Valet (1996). Results are shown in Figs. 9 and 10. Note that WEPEQ correspond to the stack of RPIs from 2 or 3 cores, except for the first 18 ka, where only the record from core MD01-2385 is used.

6. Discussion

6.1. Estimation of lock-in depth

Post-depositional remanent magnetization (pDRM) is acquired after the sediment is deposited on the seafloor and only once the lock-in depth has been reached. This phenomenon causes a mismatch between the age of sediment deposition and that of the recorded geomagnetic field, which is often younger than the surrounding sediment (e.g., Channell and Guyodo, 2013; Roberts et al., 2013; Mellström et al., 2015; Valet et al., 2017). In general, this acquisition delay is not corrected in paleomagnetic records, as it is site dependent and difficult to estimate. In addition, the magnetic records can be disturbed in the topmost first centimeters of cores as the sediment is generally not well consolidated and subject to coring disturbance. With these caveats in mind, the reliability of our high-resolution reference curve was tested over the first 10

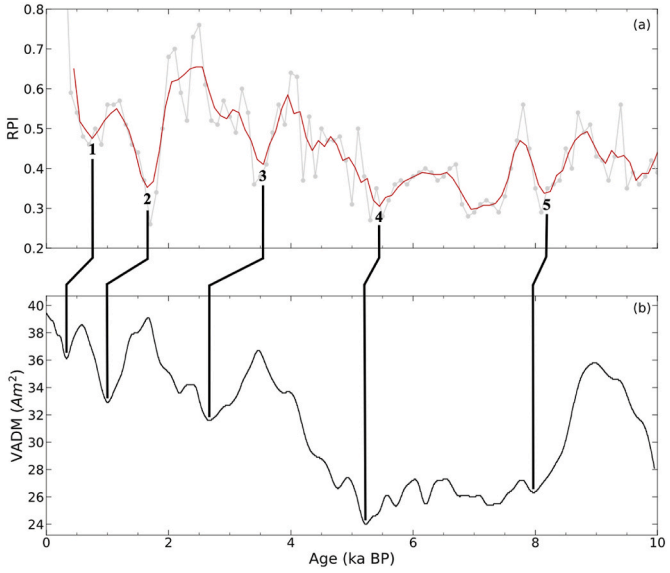

Fig. 9. (a) WEPEQ (corresponding only to data from core MD01-2385 over this time interval) and (b) CALS10k.2 model for the western equatorial pacific. The gray curve corresponds to the individual data points and the red curve is a 4-point running mean. The two curves exhibit very similar variations, highlighted by the correlation between five selected tie points, labeled 1 to 5 on the figure, corresponding to local intensity minima.

ka by comparison with a paleomagnetic field model (CALS10k.2; Constable et al., 2016). We projected the CALS10k.2 model on the MD01-2385 sampling site and extracted the VADM. Both curves are shown in Fig. 9. A strong similarity between the two curves is observed, showing nearly identical variations until 8 ka. Beyond 8 ka, the model's predictions appear slightly less accurate but the overall trend aligns between the two curves. This close match provides confidence in the reliability of our data and allows peak-to-peak comparison, which reveals a subtle but consistent shift towards older ages in the WEPEQ data, especially for the first 5 ka. As the most recent part of the CALS10k.2 model (0–5 ka) is based on a large proportion of archaeomagnetic and volcanic data for which magnetization acquisition is instantaneous, the slight temporal discrepancy between the curves is attributed to the expression of the lock-in depth of the magnetic signal. The estimated time lag between the curves remains relatively stable, of around 600 years, suggesting a lock-in depth of approximately 18 cm. This is comparable to the 20 cm proposed in other studies (Suganuma et al., 2011; Channell and Guyodo, 2013). As discussed above, the first 18 ka of WEPEQ consist exclusively of data from core MD01-2385 (see section 5). The lock-in depth defined here corresponds therefore to that of core MD01-2385, taking into account the fact that it is a site-dependent parameter. To account for the time lag induced by lock-in depth, we cautiously adjusted the RPI curves from core MD01-2385 by ~600 years towards younger ages, which represents our best lag estimate. Given that RPI curves from cores MD98-2181 and MD97-2134 were recalibrated to the age model of core MD01-2385, the WEPEQ reference curve is, by construction, also corrected for the lock-in depth effect.

6.2. Comparison with other regional reference curves

To establish inter-hemispheric and latitude variability we conducted comparisons with existing regional paleointensity stacks from marine sediments. The reference RPI stacks used here are: the regional reference curves NAPIS (La j et al., 2000), SAPIS (Stoner et al., 2002), WEPAPIS-70 (Dahrin et al., 2023), the Iberian Margin Stack (Channell et al., 2018) and the Black Sea Stack (Liu et al., 2020). We also add the high-resolution dipole moment variations inferred from measurements of the $^{10}Be/^{9}Be$ ratio around the Laschamps excursion from a Pacific

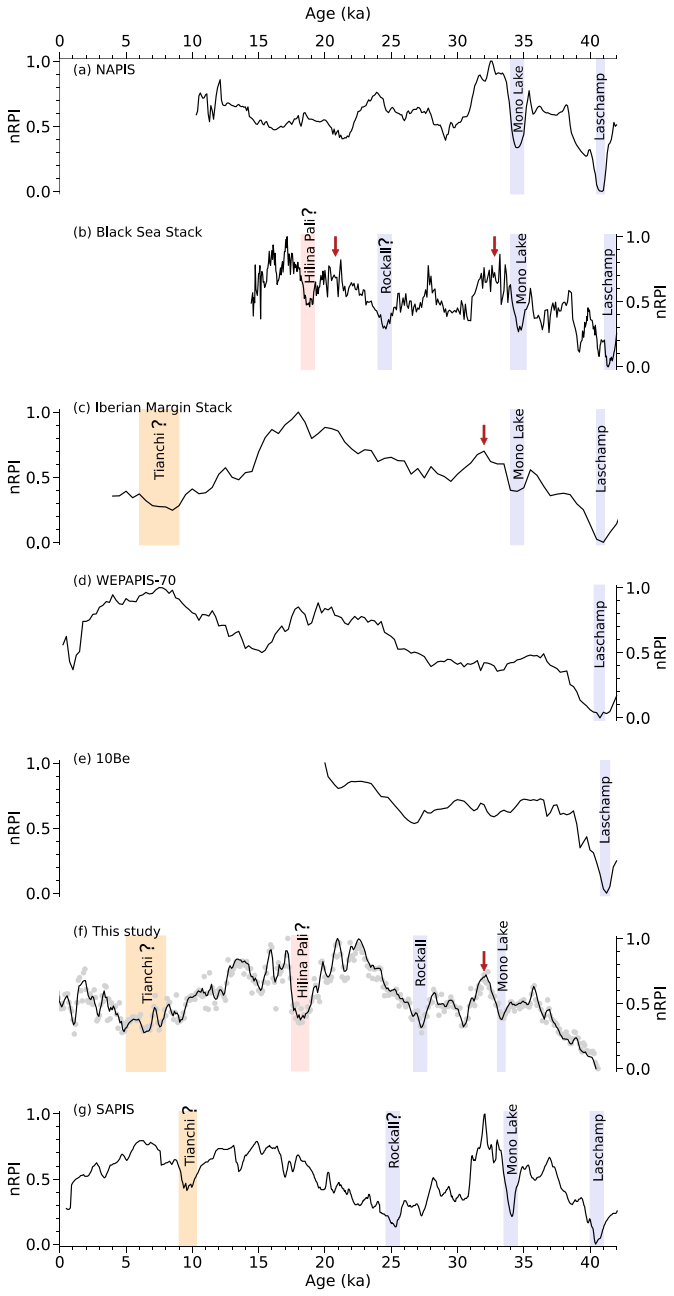

Fig. 10. Normalized relative paleointensity values (see text) of (a) NAPIS (Laj et al. 2000), (b) the Black Sea Stack (Liu et al., 2020), (c) the Iberian Margin Stack (Channell et al., 2018), (d) WEPAPIS-70 (Dahrin et al., 2023), (e) deduced from $^{10}Be/^{9}Be$ ratio (Simon et al., 2020) (f) WEPEQ (data available at https://doi.org/10.18715/IPGP.2024.ly33jn7r) and (g) SAPIS (Stoner et al., 2002). The red arrows indicate the humps discussed in the text. Intensity lows are shown by the color intervals.

equatorial marine core (Simon et al., 2020, see also Ménabréaz et al., 2012). All the curves have been normalized between 0 and 1 (0 for the lowest value, ie. the Laschamp excursion and 1 for the highest) in order to compare the paleomagnetic signal amplitude variations. The plotted curves span ages ranging from 0 to 42 ka.

From 42 ka to 35 ka, the curves are generally in good agreement with the record of the Laschamp excursion at ~41 ka followed by an increase in paleointensity with maximum values reached slightly before 35 ka. Around ~33–34 ka the Mono Lake excursion has been consistently identified in various studies (Blanchet et al., 2006; Kissel et al., 2011; Negrini et al., 2014; Liu et al., 2019) and it is clearly recorded in NAPIS,

SAPIS and the Black Sea Stack. The WEPAPIS-70 record exhibits a seemingly flat trend, which could be attributed to the low resolution of some of the curves used in this particular stack. WEPEQ and the Iberian Margin Stack showed paleointensity variations, but not the clear intensity minimum expected for the Mono Lake excursion. It is noteworthy that the cosmogenic ^{10}Be production record, considered a global indicator, did not detect the Mono Lake excursion either (see Fig. 10). Simon et al. (2020) suggest that the absence of low interval values in the geomagnetic dipole moment around 34 ka supports the hypothesis that the Mono Lake excursion has been triggered by a non-dipole field pulse instead of a significant collapse of the dipole field. Another explanation could be the short duration of this excursion, which did not lead to a cosmogenic nuclides overproduction and resulted in a smoothed record. Lastly, the lack of proportionality between measured sedimentary ^{10}Be/^{9}Be ratio and the cosmogenic ^{10}Be production has been discussed by Savranskaia et al. (2021) and could be a potential cause for the discrepancy by concealing moderate paleointensity deviations in the ^{10}Be record. Our observation of a very moderate RPI low at the scale of our sampling resolution of ~60 yr is more in favor of an event with a moderate dipole decrease and significant non dipole components with strong high latitudes influences. In such configuration the decrease of the Earth magnetic field intensity would be highly dependent on site location on the globe. Our data suggest a minimal decrease in the western Pacific equator region. This hypothesis is supported by models from Korte et al. (2019b), where the Mono Lake excursion corresponds to a regional event with strong non-dipolar contributions. Liu et al. (2020) arrived at the same conclusion using paleosecular variation records from marine sediments of the Black Sea. This emphasizes the importance of producing high-resolution, very well dated RPI curves over recent periods to access the fine scale variations and better constrain the nature of paleointensity lows, which are sometimes referred to as excursions, but fail to be detected at the global scale. Note that the Mono Lake low is followed by an intensity maximum at ~32–33 ka on all RPI stacks (with the notable exception of WEPAPIS-70) as indicated by an arrow in Fig. 10. This intensity maximum corresponds to the highest value of RPI for NAPIS and SAPIS.

During the 30–20 ka interval a faint intensity minimum has been identified on WEPEQ at around 27 ka, with a corresponding hint of intensity decrease on the ^{10}Be curve at the same age. The low relative paleointensity observed at approximately 25 ka on the Black Sea Stack and SAPIS stack could align with this intensity minimum. It could potentially correspond to the "Rockall" event dated at 26.5 ka (Channell et al., 2016). This minimum has been identified for the first time in core MD04-2822 from the Rockall Trough in the NE Atlantic, whose sedimentation rate was ~100 cm/ka over the excursion interval (Channell et al., 2016). Its duration has been estimated at around 350 years, potentially explaining its rare occurrence in marine sediments and its smoothed appearance in other records. After this event, all curves display a rather similar increasing trend from 25 to 20 ka, indicating a global phenomenon, except for the NAPIS stack, which shows RPIs decreasing until around 21 ka. During this interval spanning several thousand years, NAPIS exhibits significant discrepancies compared to all other records, including the dipole variations derived from ^{10}Be. This observation suggests that the NAPIS curve could be significantly biased by climatic factors during this interval, corresponding to the last glacial maximum.

The last 20 kyr are marked by a low RPI at ~18.5 ka which is well defined on WEPEQ and Black Sea Stack. This could correspond to the Hilina Pali event dated at ~18–19 ka (Coe et al., 1978; Leonard et al., 2017; Liu et al., 2018). This event is reported as an excursion in a few studies, for instance by Leonard et al. (2017) based on anomalous paleomagnetic directions found in ~16–~21 ka lavas from New Zealand. However, this is still much debated as it is rarely recorded in marine sediments. Only a minor RPI decrease is observed on SAPIS, WEPAPIS-70 and Iberian Margin stacks. The following RPI maximum highlighted by an arrow at ~17 ka on Fig. 10b, c and f, correspond to the highest RPI value for the Black Sea Stack and the Iberian Margin Stack. Singer et al. (2014) suggested that this "excursion" could correlate with another "excursion" that they identified in lavas from the Tianchi volcano in China and dated at ~17 ka using the ^{40}Ar/^{39}Ar method. Since then, further dating has been carried out on different crystal from the same lavas (Channell et al., 2020; Pan et al., 2022), as well as on lacustrine ash deposits from this eruption (Sun et al., 2018), leading to a revision of the age of this "excursion" towards much younger ages, around 8–10 ka. This age revision means that the presumptive Hilina Pali and Tianchi are two separate events. No clear drop in RPI is observed at 8–10 ka on the different stacks presented in Fig. 10 except for SAPIS where a low RPI is visible at ~10 ka. Note that the upper 20 ka of SAPIS should be taken cautiously because of the presence of anomalous magnetic mineralogy in three of the five stacked cores (Stoner et al., 2002). A plateau with relatively low RPIs is observed between 5 and 8 ka on WEPEQ and the Iberian Margin Stack. As discussed in section 5.2, the curve obtained in our study is in good agreement with the CALS10k.2 model, suggesting the reliability of reconstructed RPIs and the reliability of a minimum in intensity around 5–8 ka in the western Equatorial Pacific.

The majority of the so-called "excursions" discussed above correspond to moderate decreases in intensity in our reference curve, contrasting with the pronounced minima observed during the Laschamp excursion (Fig. 10). The amplitude of the signals recorded in marine sediments depends primarily on the sedimentation rate, hence the importance of obtaining high-resolution data. However, determining the average sedimentation rate and the resulting smoothing of the paleomagnetic signal for the regional RPI reference curves, which are essentially stacks, is challenging. In any case, when considering intensity lows they all appear as minor events compared to the Laschamp minima. As an example, by setting a threshold at approximately 20% of the maximum (threshold reached during the Laschamp excursion, 0.2 on the curves from Fig. 10), none of the stacks achieve values that are as low. Furthermore, the lowest values for WEPEQ are found around 5–8 ka, a period during which no significant departure from an axial dipole geometry is observed in the associated directions (Fig. 2) or reported in global models like Korte et al. (2019b). The observations mentioned above cast doubt on interpreting any of the minima as "excursions". We opt for a more cautious description, referring to them as RPI lows. This choice raises questions about whether they represent unremarkable geomagnetic secular variation events, particularly on a global scale (see also Thouveny et al., 2004).

7. Conclusions

The WEPEQ reference curve has been derived from a high-resolution paleointensity dataset with an age model resting upon a dense collection of ^{14}C dated tie-points. It has been corrected for paleomagnetic lock-in depth. WEPEQ exhibits important similarities with existing mid-latitude high-resolution stacks such as the Iberian Margin Stack and the Black Sea Stack. Minor temporal discrepancies may result from differences in the methods used for constructing the age models and the fact that the lock-in-depth was not accounted for and corrected in most datasets. The correlation is considerably weaker with sedimentary RPI records from high latitudes (notably NAPIS and, to a lesser extent, SAPIS), particularly for ages younger than 30 ka. We hypothesize that these sediment stacks, particularly those from the North Atlantic region, may be more susceptible to climatic influences, particularly ice melt events.

Due to its high-resolution nature, our reference curve exposes subtle yet distinctive variations in the relative paleointensity that suggest the emergence of non-dipole components. Notable examples include the rather moderate intensity decrease corresponding to the Mono Lake at ~34 ka, pronounced oscillation around 18.5 ka referred to as the Hilina Pali low, and low values between 5 and 8 ka, known as the Tianchi low. Our findings suggest that these intensity lows sometimes referred to as

"excursions" are local phenomena. Hence the Mono Lake can remain undetected in the western Equatorial Pacific while the Hilina Pali and Tianchi lows are prominent characteristics. These features can serve as valuable references for the region and indicators for assessing global versus local significance, as well as for refining geomagnetic models to understand the emergence of non-dipole structures. Conversely, the prolonged 5 kyr increase in paleointensity between 41 - 36 ka and 27–22 ka, as well as the humps around 32 ka, are features observed across various records and can be utilized as global reference time markers.

Declaration of competing interest

The authors declare that they have no known competing financial interests or personal relationships that could have appeared to influence the work reported in this paper.

Data availability

I have shared the link to my data at the Attach File step

Acknowledgements

We express our gratitude to Laure Meynadier for her insights provided throughout the course of this study. We thank Martine Simoes (IPGP) for discussing the complex tectonic context in Papua-New Guinea. We also thank Adriana Gonzalez Cano (IPGP) for her help with the magnetic measuring instruments and Anojh Thevarasan for his advices on the magnetic data processing, Morgane Fries (LSCE) for foraminifer controls and Jean Pascal Dumoulin for ^{14}C dating. Steve Lund and Nicolas Thouveny are thanked for providing the RPI data of core MD98-2181 and MD97-2134, respectively, and Darharta Dahrin for providing WEPAPIS-70 data. We thank two anonymous reviewers for their comments that helped to improve the manuscript. This study was funded by the European research Council (ERC) under the European Union's Seventh Framework Programme (339899 FP7/2007–2013) and by the IPGP.

Appendix A. Supplementary data

Supplementary data to this article can be found online at https://doi.org/10.1016/j.quascirev.2024.108800.

References

Baldwin, S.L., Fitzgerald, P.G., Webb, L.E., 2012. Tectonics of the new Guinea region. Annu. Rev. Earth Planet Sci. 40, 495–520. https://doi.org/10.1146/annurev-earth-040809-152540.

Blaauw, M., Christen, J.A., 2011. Flexible paleoclimate age-depth models using an autoregressive gamma process. Bayesian Anal 6. https://doi.org/10.1214/11-BA618.

Blanchet, C.L., Thouveny, N., de Garidel-Thoron, T., 2006. Evidence for multiple paleomagnetic intensity lows between 30 and 50ka BP from a western Equatorial Pacific sedimentary sequence. Quat. Sci. Rev. 25, 1039–1052. https://doi.org/10.1016/j.quascirev.2005.09.001.

Carlut, J., Quidelleur, X., Courtillot, V., Boudon, G., 2000. Paleomagnetic directions and K/Ar dating of 0 to 1 Ma lava flows from La Guadeloupe Island (French West Indies): implications for time-averaged field models. J. Geophys. Res. 105, 835–849. https://doi.org/10.1029/1999JB900238.

Channell, J.E.T., 2013. Biogenic magnetite, detrital hematite, and relative paleointensity in Quaternary sediments from the Southwest Iberian Margin. Earth Planet Sci. Lett. 11.

Channell, J.E.T., Guyodo, Y., 2013. The Matuyama chronozone at ODP site 982 (Rockall bank): evidence for decimeter-scale magnetization lock-in depths. In: Channell, J.E.T., Kent, D.V., Lowrie, W., Meert, J.G. (Eds.), Geophysical Monograph Series. American Geophysical Union, pp. 205–219. https://doi.org/10.1029/145GM15.

Channell, J.E.T., Harrison, R.J., Lascu, I., McCave, I.N., Hibbert, F.D., Austin, W.E.N., 2016. Magnetic record of deglaciation using FORC-PCA, sortable-silt grain size, and magnetic excursion at 26 ka, from the Rockall Trough (NE Atlantic): a magnetic record of deglaciation. G-cubed 17, 1823–1841. https://doi.org/10.1002/2016GC006300.

Channell, J.E.T., Hodell, D.A., Crowhurst, S.J., Skinner, L.C., Muscheler, R., 2018. Relative paleointensity (RPI) in the latest Pleistocene (10–45 ka) and implications for deglacial atmospheric radiocarbon. Quat. Sci. Rev. 191, 57–72. https://doi.org/10.1016/j.quascirev.2018.05.007.

Channell, J.E.T., Singer, B.S., Jicha, B.R., 2020. Timing of Quaternary geomagnetic reversals and excursions in volcanic and sedimentary archives. Quat. Sci. Rev. 228, 106114 https://doi.org/10.1016/j.quascirev.2019.106114.

Channell, J.E.T., Vázquez Riveiros, N., Gottschalk, J., Waelbroeck, C., Skinner, L.C., 2017. Age and duration of Laschamp and Iceland basin geomagnetic excursions in the South atlantic ocean. Quat. Sci. Rev. 167, 1–13. https://doi.org/10.1016/j.quascirev.2017.04.020.

Channell, J.E.T., Xuan, C., Hodell, D.A., 2009. Stacking paleointensity and oxygen isotope data for the last 1.5 Myr (PISO-1500). Earth Planet Sci. Lett. 283, 14–23. https://doi.org/10.1016/j.epsl.2009.03.012.

Coe, R.S., Grommé, S., Mankinen, E.A., 1978. Geomagnetic paleointensities from radiocarbon-dated lava flows on Hawaii and the question of the Pacific nondipole low. J. Geophys. Res. 83, 1740–1756. https://doi.org/10.1029/JB083iB04p01740.

Constable, C., Korte, M., Panovska, S., 2016. Persistent high paleosecular variation activity in southern hemisphere for at least 10 000 years. Earth Planet Sci. Lett. 453, 78–86. https://doi.org/10.1016/j.epsl.2016.08.015.

Dahrin, D., Harlianti, U., Bijaksana, S., Kirana, K.H., Fajar, S.J., Suryanata, P.B., 2023. WEPAPIS 70 (Western Pacific paleointensity-stacking for the last 70 ka). Quat. Sci. Rev. 315, 108232 https://doi.org/10.1016/j.quascirev.2023.108232.

Franke, J., Paul, A., Schulz, M., 2008. Modeling variations of marine reservoir ages during the last 45 000 years. Clim. Past.

Goto, R., Yamazaki, T., Okutsu, N., Ashi, J., 2024. Geomagnetic relative paleointensity and direction during the last 40,000 years obtained from a sediment core in the Nankai Trough. Earth Planets Space 76, 4. https://doi.org/10.1186/s40623-023-01945-x.

Guyodo, Y., Valet, J.-P., 1999. Global changes in intensity of the Earth's magnetic field during the past 800 kyr. Nature 399, 249–252. https://doi.org/10.1038/20420.

Guyodo, Y., Valet, J.-P., 1996. Relative variations in geomagnetic intensity from sedimentary records: the past 200,000 years. Earth Planet Sci. Lett. 143, 23–36. https://doi.org/10.1016/0012-821X(96)00121-5.

King, J.W., Banerjee, S.K., Marvin, J., 1983. A new rock-magnetic approach to selecting sediments for geomagnetic paleointensity studies: application to paleointensity for the last 4000 years. J. Geophys. Res. 88, 5911–5921. https://doi.org/10.1029/JB088iB07p05911.

Kissel, C., Guillou, H., Laj, C., Carracedo, J.C., Nomade, S., Perez-Torrado, F., Wandres, C., 2011. The Mono Lake excursion recorded in phonolitic lavas from Tenerife (Canary Islands): paleomagnetic analyses and coupled K/Ar and Ar/Ar dating. Phys. Earth Planet. In. 187, 232–244. https://doi.org/10.1016/j.pepi.2011.04.014.

Korte, M., Brown, M.C., Gunnarson, S.R., Nilsson, A., Panovska, S., Wardinski, I., Constable, C.G., 2019a. Refining Holocene geochronologies using palaeomagnetic records. Quat. Geochronol. 50, 47–74. https://doi.org/10.1016/j.quageo.2018.11.004.

Korte, M., Brown, M.C., Panovska, S., Wardinski, I., 2019b. Robust characteristics of the Laschamp and Mono Lake geomagnetic excursions: results from global field models. Front. Earth Sci. 7, 86. https://doi.org/10.3389/feart.2019.00086.

La j, C., Kissel, C., Mazaud, A., Channell, J.E.T., Beer, J., 2000. North Atlantic palaeointensity stack since 75ka (NAPIS–75) and the duration of the Laschamp event. Philos. Trans. R. Soc. London, Ser. A: Math. Phys. Eng. Sci. 358, 1009–1025. https://doi.org/10.1098/rsta.2000.0571.

Laj, C., Guillou, H., Kissel, C., 2014. Dynamics of the earth magnetic field in the 10–75 kyr period comprising the Laschamp and Mono Lake excursions: New results from the French Chaîne des Puys in a global perspective. Earth Planet Sci. Lett. 387, 184–197. https://doi.org/10.1016/j.epsl.2013.11.031.

Laj, C., Kissel, C., Beer, J., 2013. High resolution global paleointensity stack since 75 kyr (GLOPIS-75) calibrated to absolute values. In: Channell, J.E.T., Kent, D.V., Lowrie, W., Meert, J.G. (Eds.), Geophysical Monograph Series. American Geophysical Union, pp. 255–265. https://doi.org/10.1029/145GM19.

Larrasoaña, J.C., Roberts, A.P., Stoner, J.S., Richter, C., Wehausen, R., 2003. A new proxy for bottom-water ventilation in the eastern Mediterranean based on diagenetically controlled magnetic properties of sapropel-bearing sediments. Palaeogeogr. Palaeoclimatol. Palaeoecol. 190, 221–242. https://doi.org/10.1016/S0031-0182(02)00607-7.

Leonard, G.S., Calvert, A.T., Hopkins, J.L., Wilson, C.J.N., Smid, E.R., Lindsay, J.M., Champion, D.E., 2017. High-precision 40Ar/39Ar dating of Quaternary basalts from Auckland Volcanic Field, New Zealand, with implications for eruption rates and paleomagnetic correlations. J. Volcanol. Geoth. Res. 343, 60–74. https://doi.org/10.1016/j.jvolgeores.2017.05.033.

Levi, S., Banerjee, S.K., 1976. On the possibility of obtaining relative paleointensities from lake sediments. Earth Planet Sci. Lett. 29, 219–226. https://doi.org/10.1016/0012-821X(76)90042-X.

Liu, J., Nowaczyk, N., Frank, U., Arz, H., 2019. Geomagnetic paleosecular variation record spanning from 40 to 20 ka – implications for the Mono Lake excursion from Black Sea sediments. Earth Planet Sci. Lett. 509, 114–124. https://doi.org/10.1016/j.epsl.2018.12.029.

Liu, J., Nowaczyk, N.R., Panovska, S., Korte, M., Arz, H.W., 2020. The Norwegian-Greenland Sea, the Laschamps, and the Mono Lake excursions recorded in a Black Sea sedimentary sequence spanning from 68.9 to 14.5 ka. JGR Solid Earth 125, e2019JB019225. https://doi.org/10.1029/2019JB019225.

Lund, S., Schwartz, M., Stott, L., 2017. Long-term paleomagnetic secular variation and excursions from the western equatorial pacific ocean (MIS2-4). Geophys. J. Int. ggx029. https://doi.org/10.1093/gji/ggx029.

Mellström, A., Nilsson, A., Stanton, T., Muscheler, R., Snowball, I., Suttie, N., 2015. Post-depositional remanent magnetization lock-in depth in precisely dated varved

sediments assessed by archaeomagnetic field models. Earth Planet Sci. Lett. 410, 186–196. https://doi.org/10.1016/j.epsl.2014.11.016.

Ménabréaz, L., Bourlès, D.L., Thouveny, N., 2012. Amplitude and timing of the Laschamp geomagnetic dipole low from the global atmospheric ^{10}Be overproduction: contribution of authigenic ^{10}Be/^{9}Be ratios in west equatorial Pacific sediments: MAGNETIC MODULATION OF ^{10}Be PRODUCTION. J. Geophys. Res. 117 https://doi.org/10.1029/2012JB009256.

Negrini, R.M., McCuan, D.T., Horton, R.A., Lopez, J.D., Cassata, W.S., Channell, J.E.T., Verosub, K.L., Knott, J.R., Coe, R.S., Liddicoat, J.C., Lund, S.P., Benson, L.V., Sarna-Wojcicki, A.M., 2014. Nongeocentric axial dipole field behavior during the Mono Lake excursion. JGR Solid Earth 119, 2567–2581. https://doi.org/10.1002/2013JB010846.

Olson, P., Reynolds, E., Hinnov, L., Goswami, A., 2016. Variation of ocean sediment thickness with crustal age. G-cubed 17, 1349–1369. https://doi.org/10.1002/2015GC006143.

Orynbaikyzy, A., Plank, S., Vetrita, Y., Martinis, S., Santoso, I., Dwi Ismanto, R., Chusnayah, F., Tjahjaningsih, A., Genzano, N., Marchese, F., Rokhis Khomarudin, M., Strunz, G., 2023. Joint use of Sentinel-2 and Sentinel-1 data for rapid mapping of volcanic eruption deposits in Southeast Asia. Int. J. Appl. Earth Obs. Geoinf. 116, 103166 https://doi.org/10.1016/j.jag.2022.103166.

Pan, B., De Silva, S.L., Danisík, M., Schmitt, A.K., Miggins, D.P., 2022. The Qixiangzhan eruption, Changbaishan-Tianchi volcano, China/DPRK: new age constraints and their implications. Sci. Rep. 12, 22485 https://doi.org/10.1038/s41598-022-27038-5.

Roberts, A.P., Tauxe, L., Heslop, D., 2013. Magnetic paleointensity stratigraphy and high-resolution Quaternary geochronology: successes and future challenges. Quat. Sci. Rev. 61, 1–16. https://doi.org/10.1016/j.quascirev.2012.10.036.

Savranskaia, T., Egli, R., Valet, J.-P., Bassinot, F., Meynadier, L., Bourlès, D.L., Simon, Q., Thouveny, N., 2021. Disentangling magnetic and environmental signatures of sedimentary 10Be/9Be records. Quat. Sci. Rev. 257, 106809 https://doi.org/10.1016/j.quascirev.2021.106809.

Simon, Q., Thouveny, N., Bourlès, D.L., Valet, J.-P., Bassinot, F., 2020. Cosmogenic 10Be production records reveal dynamics of geomagnetic dipole moment (GDM) over the Laschamp excursion (20–60 ka). Earth Planet Sci. Lett. 550, 116547 https://doi.org/10.1016/j.epsl.2020.116547.

Singer, B.S., Jicha, B.R., He, H., Zhu, R., 2014. Geomagnetic field excursion recorded 17 ka at Tianchi Volcano, China: new ^{40}Ar/^{39}Ar age and significance. Geophys. Res. Lett. 41, 2794–2802. https://doi.org/10.1002/2014GL059439.

Stoner, J.S., Channell, J.E.T., Hillaire-Marcel, C., Kissel, C., 2000. Geomagnetic paleointensity and environmental record from Labrador Sea core MD95-2024: global marine sediment and ice core chronostratigraphy for the last 110 kyr. Earth Planet Sci. Lett. 183, 161–177. https://doi.org/10.1016/S0012-821X(00)00272-7.

Stoner, J.S., Laj, C., Channell, J.E.T., Kissel, C., 2002. South Atlantic and North Atlantic geomagnetic paleointensity stacks (0–80ka): implications for inter-hemispheric correlation. Quat. Sci. Rev. 21, 1141–1151. https://doi.org/10.1016/S0277-3791(01)00136-6.

Stuiver, M., Reimer, P.J., 1993. Extended ^{14}C data base and revised CALIB 3.0 ^{14}C age calibration program. Radiocarbon 35, 215–230. https://doi.org/10.1017/S0033822200013904.

Suganuma, Y., Okuno, J., Heslop, D., Roberts, A.P., Yamazaki, T., Yokoyama, Y., 2011. Post-depositional remanent magnetization lock-in for marine sediments deduced from 10Be and paleomagnetic records through the Matuyama–Brunhes boundary. Earth Planet Sci. Lett. 311, 39–52. https://doi.org/10.1016/j.epsl.2011.08.038.

Sun, C., Wang, L., Plunkett, G., You, H., Zhu, Z., Zhang, L., Zhang, B., Chu, G., Liu, J., 2018. Ash from the changbaishan qixiangzhan eruption: a new early Holocene marker horizon across east asia. JGR Solid Earth 123, 6442–6450. https://doi.org/10.1029/2018JB015983.

Tauxe, L., 1993. Sedimentary records of relative paleointensity of the geomagnetic field: theory and practice. Rev. Geophys. 31, 319. https://doi.org/10.1029/93RG01771.

Thouveny, N., Carcaillet, J., Moreno, E., Leduc, G., Nérini, D., 2004. Geomagnetic moment variation and paleomagnetic excursions since 400 kyr BP: a stacked record from sedimentary sequences of the Portuguese margin. Earth Planet Sci. Lett. 219, 377–396. https://doi.org/10.1016/S0012-821X(03)00701-5.

Valet, J.-P., Meynadier, L., Guyodo, Y., 2005. Geomagnetic dipole strength and reversal rate over the past two million years. Nature 435, 802–805. https://doi.org/10.1038/nature03674.

Valet, J.-P., Tanty, C., Carlut, J., 2017. Detrital magnetization of laboratory-redeposited sediments. Geophys. J. Int. 210, 34–41. https://doi.org/10.1093/gji/ggx139.

Wu, Q., Colin, C., Liu, Z., Bassinot, F., Dubois-Dauphin, Q., Douville, E., Thil, F., Siani, G., 2017. Foraminiferal εNd in the deep north-western subtropical Pacific Ocean: tracing changes in weathering input over the last 30,000 years. Chem. Geol. 470, 55–66. https://doi.org/10.1016/j.chemgeo.2017.08.022.